

Multi-Point Magnetospheric Reconnaissance Imaging: Visualization of Ion Dynamics, Evolution, Origins, and Structure

D. G. Mitchell¹, H. O. Funsten², M. Gruntman³, M. Hesse⁴, B. H. Mauk¹, R. R. Meier⁵, D. J. McComas⁶, E. C. Roelof¹, and E. E. Scime⁶

1. Introduction

With the selection of IMAGE for the NASA MIDEX Program, magnetospheric imaging is a measurement approach whose time has come. It is, therefore, appropriate that we begin the development of the next generation of instrumentation, techniques, and mission design so that its vast potential may be realized in full. The most obvious and significant improvement will be to image the magnetosphere from multiple vantage points. With *in-situ* measurements, the addition of more spacecraft adds only more individual samples within the vast volume of the magnetosphere. With magnetospheric imaging, the addition of incrementally more vantage points improves our ability to extract the 3-D structure of the global magnetospheric system in a qualitatively different way.

We are currently working on a program called Multi-Point Magnetospheric Reconnaissance Imaging: Visualization of Ion Dynamics, Evolution, Origins, and Structure (MRI-VIDEOS), to develop a mission concept or concepts by which, for a minimum expenditure, an optimized configuration of spacecraft for multi-point magnetospheric imaging can be deployed. Four tasks were proposed:

(1) Design to cost (different missions on leave for different cost envelopes). (2) Refinement of multi-point image inversion techniques, for assessment of science return. (3) Conceptual design of super-low cost, autonomous imaging spacecraft. (4) Refinement and assessment of magnetospheric imaging techniques. This paper reports on progress on task (2), which helps constrain tasks (1), (3) and (4).

2. Magnetospheric Imaging—Techniques

There are two promising techniques for imaging the 3D magnetospheric plasma that have been experimentally verified on spacecraft. One is the imaging of hot plasma regions by detection of energetic neutral atoms. Energetic neutral atoms, or ENA, are generated when singly charged, energetic ions (<1 keV to ~1 MeV) undergo charge exchange with ambient cold neutral gases (Roelof et al., 1985; Roelof, 1987; Roelof et al., 1996; Lui et al., 1996; Henderson et al., 1997). The other primary technique discussed here is the imaging of the plasmasphere by detection of extreme ultraviolet light. He II 30.4nm EUV light is re-radiated by plasmaspheric He⁺ after resonant absorption of the solar 30.4nm line (Meier and Weller, 1972).

3. Magnetospheric Imaging—Multiple Vantage Points

A frequently voiced criticism of magnetospheric imaging is that the interpretation of the images will be very difficult, and severely model-

dependent. This is mostly because for a magnetospheric image, whether in ENA or in EUV light, the emission regions are optically thin. Therefore, the image is a projection onto a 2-D plane of the 3-D emission structure of the magnetosphere. Interpretation of the image requires constraining the position of the emission along the line of sight by the known physics of the magnetosphere, for example, Liouville's theorem that constrains the distribution of particle phase space density along the lines of magnetic force. Still, some structures will remain without question uninterpretable. A similar difficulty is encountered in the interpretation of medical x-ray images, where one is imaging a 3-D, optically thin object (the human body) collapsed onto a two-dimensional plane. In the case of x-rays, it is relatively simple to interpret certain high contrast features of the 2-D image, based on prior understanding of anatomy, while other features are nearly impossible to interpret without using a multi-point imaging approach, e.g. the CAT scan and magnetic resonance imaging.

This limitation of single vantage point imaging can, however, be readily mitigated by an approach analogous to the CAT scan. Image interpretation can be made far less model dependent through the use of multiple imaging platforms. Multi-point viewing will greatly improve the determination of such basic parameters as the L-shell, which dominates the emission, the azimuthal distribution of plasma along the L-shell, the pitch-angle distribution of the plasma ions, and the departure of the plasma contained by the magnetic field from a dipole configuration. The migration of plasma from the plasmasphere to the magnetosphere in the form of plasma blobs or Sun-directed tails could be discerned unambiguously from multi-point imaging. In fact, the optically thin nature of the emission becomes a distinct advantage for multipoint imaging, since the entire three-dimensional volume may be imaged.

Thus the most important contribution to magnetospheric science that is offered by a multipoint magnetospheric imaging mission is its ability to unambiguously determine the connectivity and causal relationships between the different regions, by locating the ENA or EUV emission regions with a precision not possible from a single vantage point.

4. Image Deconvolution

Figure 1 provides a very simple illustration for why multi-point imaging is so advantageous. The two simulated ENA images (30 to 50 keV neutral hydrogen in a magnetotail region between $X = -5 R_E$ and $X = -12 R_E$) are based on a magnetotail model which has complete symmetry in Y and Z. The view from above (top panel) shows that symmetry. However, an oblique view produces an asymmetric image. On the basis of that image alone, it would be very difficult to tell if there was a true asymmetry in the plasma distribution or not. The last panel shows geometrically why the oblique view is not symmetric, but without multi-point imaging, the data would be too underdetermined to unfold the structure.

Fundamental to any image unfolding technique for magnetospheric images is the order imposed upon the particle distributions by the mag-

¹The Johns Hopkins University, Applied Physics Laboratory, Laurel, Maryland

²Space and Atmospheric Sciences Group, Los Alamos, NM

³Space Sciences Center, University of Southern California, Los Angeles, CA

⁴NASA, Goddard Space Flight Center, Greenbelt, MD

⁵Naval Research Laboratory, Washington, D.C.

⁶West Virginia University, Morgantown, WV

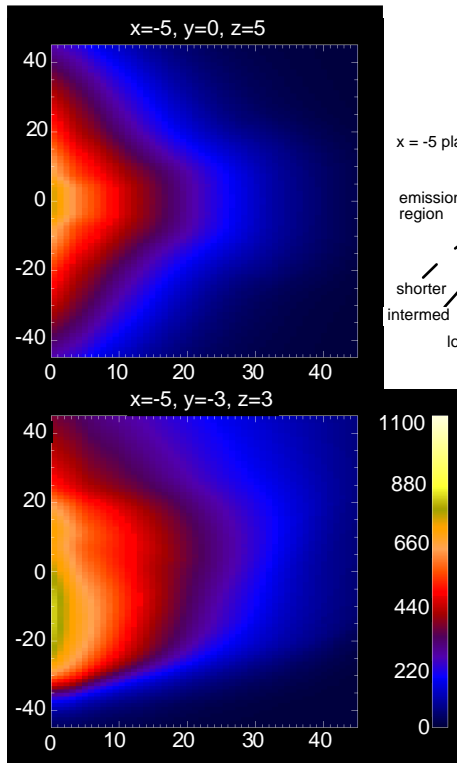


Figure 1. The same model magnetotail viewed from two locations. The combination of the two images shows that the asymmetry is caused by the viewing geometry, as illustrated in the sketch to the right.

netic field lines. The ion distributions are not a random function in three dimensions, but rather are well ordered in the *two* dimensional space of L (the McIlwain parameter) and magnetic longitude F (or magnetic local time—MLT). The third magnetospheric coordinate Λ (invariant latitude) is ignorable for energetic ions (in the absence of strong scattering), because ring current intensities can be mapped from the equator along a flux tube using the first adiabatic invariant. The latitude mapping is less well known for the suprathermal He^+ in the plasmasphere, but the Λ -dependence is the weakest of the three variables.

5. Multiple Vantage Point ENA Image Analysis

The widely different ways in which the distribution of energetic ions can be encoded into ENA images is demonstrated vividly in Figure 2. Here, the same ion distribution (to be described in more detail below) is imaged from four positions along a polar orbit (apogee= $8 R_E$ geocentric, perigee=1000 km altitude). All positions are in the dawn geomagnetic meridian. The radii and geomagnetic latitudes are: $1.2 R_E$, S68°; $4.3 R_E$, N45°; $6.5 R_E$, N68°; $8.0 R_E$, N89°; Magnetic north is towards the tops of the images, and the sun is to the right. The projection is a 90° half-width fish-eye, i.e., the hemisphere centered on the center of the Earth (solid black circle). The pixel count rates (and simulated Poisson counting fluctuations) are representative of the injection phase for a moderate geomagnetic storm as imaged in a one-minute exposure of 20–30 keV H atoms by an instrument like the MENA system on the IMAGE mission which can resolve $4^\circ \times 4^\circ$ pixels. The color bar is logarithmic, covering a factor of 100 in counts/

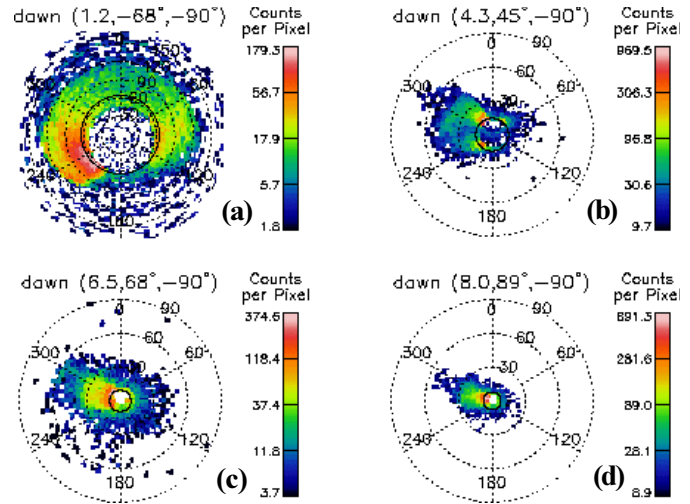


Figure 2. Four simulated ENA images with Poisson statistics as seen from vantage points in the dawn meridian. All were generated from the same non-parametric ion distribution. These images were used as the inputs to the parameter extraction algorithms.

pixel.

Anyone not familiar with ENA imaging would find it difficult to accept that these images are all of the same ion distribution. It is often commonly assumed that a view from a high altitude apogee is ideal for interpreting ENA images, and little attention has been given to the potential for low altitude (or perigee) imaging. The polar view in Fig. 2d certainly reveals the longitude dependence of the ion distribution; it is most intense at 2200 MLT. However, note that the outer extent in L is not that well defined. At the larger radii, the counts are low, because there is a relatively low density of the cold neutral H-atom geocorona, so the outer limits of the L -dependence of the ion distribution are unclear in this one-minute exposure. In principle, one could also identify the large- L limits from the boundaries of the dark (non-emitting) polar cap on the Earth. However, even though the pixel counts are among the highest in this polar region, the pixel size is too small to resolve details of the L -dependence from a radius of $8 R_E$. On the other hand, consider the image from near perigee in Figure 2a. There, the angular resolution is excellent around the polar cap, and moreover the outer extremes of the populated L -shells are now viewed edge-on at radii $r < L$, where the geocoronal H-atom density is higher than at $r = L$. That is why the outer edges are imaged with more contrast, and the closer distance to them also yields better spatial resolution from the fixed pixel size. The price one pays for a perigee view is the obscuration of a sizable portion of the magnetosphere by the Earth itself.

So which view point is “better”? Clearly there are advantages and disadvantages to every choice. We can address this question in a more quantitative manner by applying an automated extraction algorithm to the simulated images in Figure 2, and seeing which view (or which combination of views) re-constructs the input ion distribution most faithfully. The extraction technique is a minimization of the χ^2 measure of the differences between the pixel counts and those calculated from a parametric model of the ion distribution. A hierarchy of minimization techniques is utilized; details are given in Roelof and Skinner [Space Sci. Rev., submitted 1998]. In this example, the model for the ion distribution optimized 36 parameters. The results are presented in Figure 3 which shows the L -MLT plots of the input ion distributions.

Figure 3a is the actual input distribution. Noon is at the top of the

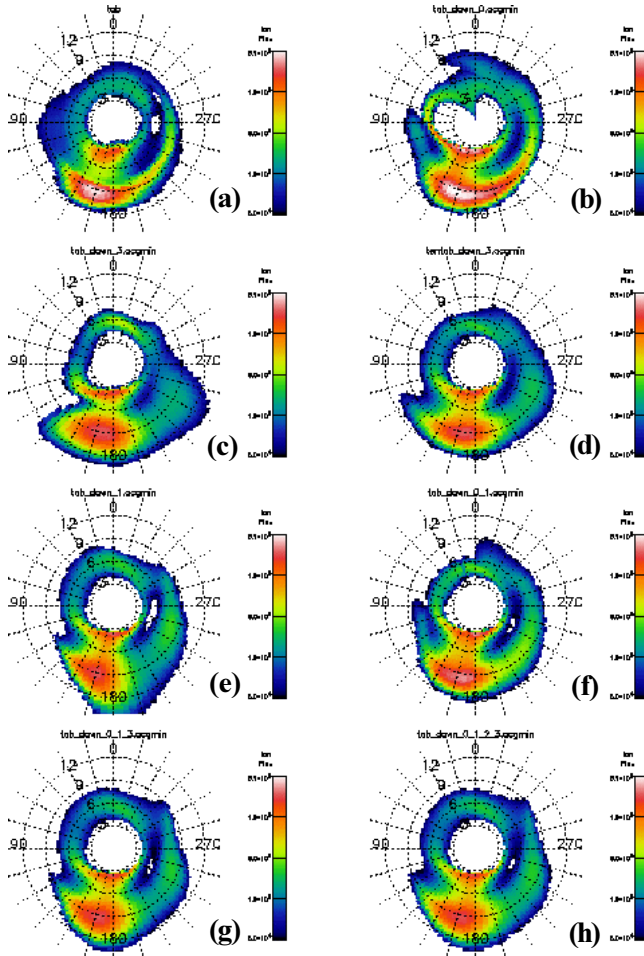


Figure 3. Eight ion distributions in the L-phi plane. The upper left distribution shows the non-parametric distribution used to generate all the ENA images. The remaining seven distributions are the result of the parameter extractions using various permutations of vantage points and exposure times. They can be compared to the input distribution to assess the success of the extraction using specific vantage point(s). From left to right, top to bottom: non-parametric input ion distribution, result from Mlat 68S, result from Mlat 89N, result from Mlat 89N with ten minute exposure, result from Mlat 45N, result from Mlat 68S and 45N, result from Mlat 68S, 45N, and 89N, and result from all four vantage points (Mlat 68S, 45N, 68N, 89N).

plots, and $L=\text{constant}$ dashed circles are plotted every $3 R_E$. The input distribution is created non-parametrically (independent of the model used in the minimization algorithm). One sees an outer injection at 2200 MLT and $L\sim 7$, an inner maximum at the same MLT, and a residual of convection from a prior injection extending around from the dawn meridian. Figure 3b (upper right) is the ion distribution extracted from the perigee image (Figure 2a). Figure 3c is extracted from the polar view (Figure 2d), and Figure 3d is the from the same position, but with a 10 minute, rather than a one minute exposure time (to reduce the counting statistics in the pixels viewing the outer L-shells). Figure 3e is obtained from the N45° position (Figure 2b), while Figure 3f is extracted simultaneously from the S68° and N45° pair of images. Likewise, Figure 3g uses triple viewpoints (S65°, N45°, N89°) while Figure 3h uses all four vantage points (S65°, N45°, N68°, N89°). While all the extracted distributions obtain the essential location of the injection maximum, only the extractions that used the near-perigee

(S68°) viewpoint obtained the lower intensity detailed.

We must not be too hasty in drawing overly generalized conclusions from this one set of examples. We are justified in saying that the broad features of the ion distribution can be extracted from any of the single images, and we can go a bit further and say that if the perigee image views one of the less intense structures clearly (as we did here with the convection feature extending from midnight to dawn), then the perigee view is quite valuable in reconstructing these structures correctly.

To make a final point concerning multiple viewpoint ENA imaging, we present in Figure 4 a true low-Earth orbit image of the same ion distribution viewed from 640 km. The spacecraft is at N80° latitude on the midnight meridian, and the view is a hemisphere (as before) looking down 10° from the anti-sun direction. The angular resolution of the plot is $1^\circ \times 1^\circ$. The upper (tangent) edge of the populated L-shells is easily identified, as is the emission maximum from the injection centered on 2200 MLT. What is new here is the very intense emission below the lines of sight to the Earth's limb (solid black curve). Note that the color bar here covers logarithmically a factor of 10,000 (vs. 100 in Figure 2). This emission comes from the interaction of nearly mirroring energetic ions with the exobase populations of atomic O and He. The simulation is based on the mathematical formulation of this exospheric ENA emission given by Roelof [1997b], motivated by the limb emissions detected by the Swedish micro-satellite "Astrid" [C:son Brandt et al., submitted to JGR, 1998]. Figure 4 dramatically demonstrates the powerful role that could be played by a low-Earth orbiting ENA imager. The very bright ENA emission from the exobase allows excellent resolution of ion injection events both temporally and spatially (in MLT). When complemented by the global views of the complete L-shells obtainable from high-altitude imagers, the full spatial and temporal picture can be unfolded [Roelof, 1997a].

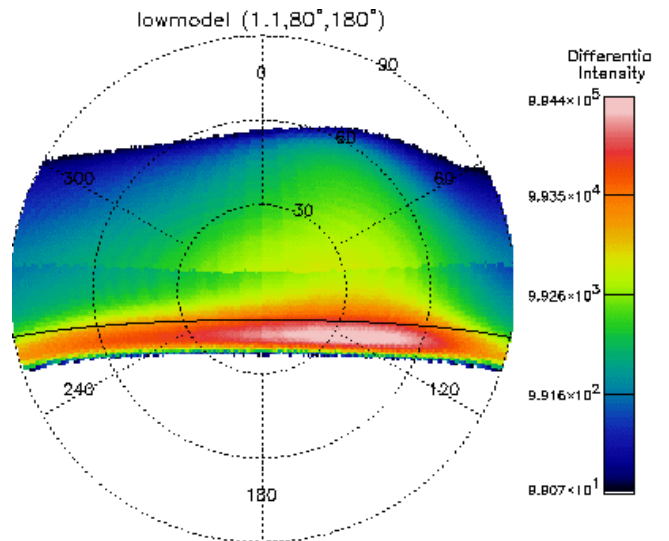


Figure 4. Simulated low altitude ENA image as seen from the midnight meridian. The image was generated from the same non-parametric ion distribution used to generate the four images in Figure 2). However, in this version of the model, the gyrating ions are attenuated as they travel along a field line and the emergent ENA is also attenuated. There is also a pitch angle anisotropy introduced for high L-shells ($L > 6$) in which the loss cone is filled. Neither an instrument response nor Poisson statistics were applied.

6. Multipoint EUV Imaging

The plasmasphere, interposed between the ionosphere and the magnetosphere, is controlled by complex processes originating in both regions. The plasmopause, the outer boundary of the plasmasphere, is where co-rotating plasma from the ionosphere encounters the convection electric field that is generated by the flow of the solar wind across the magnetosphere. The basic features of the plasmasphere have been known since the early 1960's, but many fundamental properties are still not understood [Carpenter, 1995]. Some open questions are: What is the instantaneous global shape of the plasmopause? How does it evolve in response to enhanced convection electric field activity? How are discrete plasma structures beyond the plasmopause formed and how do they evolve? How does the excess plasma flow from the ionosphere escape to the magnetosphere? What are the physical processes which are behind the plasmopause reformation during active conditions?

Global "snapshots" of the plasmasphere from high Earth orbit are essential to answer these questions. Remote sensing is the only way to address these global issues. Observations of the plasmasphere in the light of He⁺ 30.4 nm resonance radiation makes remote sensing possible because He⁺ follows the total plasma density in the plasmasphere [Horwitz et al., 1990; Craven et al., 1997]. The plasmaspheric remote sensing concept was discovered with an NRL rocket experiment [Johnson et al., 1971] and has been validated through a number of low altitude satellite and rocket measurements of the plasmasphere from the "inside out" [Williams et al., 1992]. In the future, imagers positioned outside the plasmasphere will provide a powerful new capability to see the global character of the plasmasphere for the first time.

Lacking so far in the evolution of plasmaspheric imaging concepts is a demonstration that relevant plasmaspheric parameters can be retrieved from such data. Actual tomography is difficult due to the number of spacecraft needed for complete sampling of every volume element. As an alternative, we have developed a formalism for inverting plasmaspheric remote sensing data based on the principles of Discrete Inverse Theory (DIT; see Tarantola [1987], Menke [1989], and Picone et al. [1997]). The inversion process begins with discrete data, a parameterized forward model of those data, and a method of retrieving the parameters and their uncertainties from the data. Thus, a priori information is introduced in the form of a model (ideally based on physics) containing parameters which can be retrieved from data. Our approach is to use the iterative maximum likelihood method to minimize the generalized χ^2 , thereby producing optimal estimates of the model parameters.

7. STP 72-1 Analysis

The first application of the new methodology to plasmaspheric remote sensing was the inversion of He⁺ 30.4 nm intensities observed from the low Earth orbiting (LEO) STP 72-1 satellite, launched in October 1972 [Meier et al., 1998]. Intensities were measured in the near-zenith direction from 750 km, as a function of satellite orbital angle. STP 72-1 was in a sun-synchronous, 98.3 deg inclination orbit, with the Sun-Earth line constrained to the orbital plane. The STP 72-1 data were inverted using a five parameter model of the helium ion concentration (see Meier et al. [1988] for details). The first two parameters were the plasmopause L-shell and a scalar of the magnitude of the intensity. An analytic function containing the three additional parameters described the variation of the density with altitude for various L-shells. This parameterization was derived from first principles FLIP model runs [Newberry et al., 1989]. An example of the optimal

fit to a night portion of an STP orbital pass is shown in Figure 5, along with the retrieved He⁺ densities. While excellent fits to the observed intensities were obtained, large uncertainties were found in the retrieved helium ion densities. Even so, the plasmopause L-shell was retrieved with good precision, of order few per cent.

To investigate the cause of the uncertainties in the retrieved model parameters, Meier et al. [1998] developed an ansatz in which synthetic remote sensing data are created using known input parameters. Instrumental Gaussian noise is included using an assumed conversion from intensity (in Rayleighs) to counts. The retrieval process is then applied to the artificial data and optimal estimates of the parameters

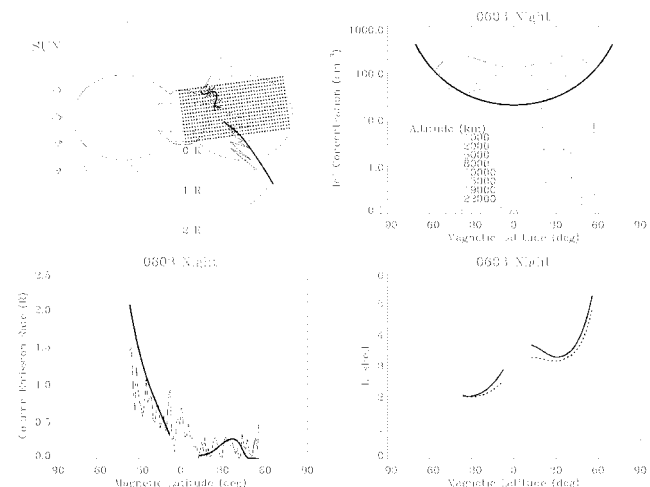


Figure 5. Comparison of model emission rates to nighttime data from orbit 603 on November 15, 1972. Upper left panel shows meridional plot where intensity is plotted radially outward along the satellite track, which coincides with the 0 R circle. Model results are given by smooth curve. Lower left shows model-data comparison in rectilinear format. The shaded region covers contaminated data which were not included in the analysis. Individual data points connected by dotted line. Upper right panel shows He⁺ concentrations versus magnetic latitude for selected altitudes. Lower right panel shows L-shell where instrument line of sight breaks into sunlight. The solid line gives the L-shell of the center of the instrument FOV, while the dotted line indicates the lowest sunlit L-shell which is seen within the full 9° FOV. For further details see Meier et al. [1998].

are obtained. Since the "true" parameters are known, the quality of the optimal estimates can be studied. Two key tools for establishing the quality of retrieved model parameters for a particular observational scenario are the covariance matrix and the model resolution matrix [Menke, 1989; Meier et al., 1998]. Parameter variances are contained in the diagonal elements of the covariance matrix and the off-diagonal elements are related to correlations among parameters. The model resolution matrix determines how well the retrieved model parameters match the "true" values. If the model resolution matrix, R [Menke, 1989], equals the identity matrix, I (i.e., unity diagonal elements and very small off-diagonal elements), the observational scenario contains sufficient information to retrieve the model parameters. However, other factors such as poor counting statistics may preclude retrievals with high precision. The diagonal elements of the covariance matrix contain that information. Uncertainties in helium ion densities can be calculated from uncertainties in model parameters using the standard propagation of errors formula (Equation 13 of Meier et al. [1998]).

The DIT tools described above were used to analyze the model parameters retrieved from the STP data. The analysis showed that

while low count rates contributed to parameter uncertainties, the principal source of error was the lack of sufficient sampling of the plasmasphere. Investigation of alternative observing scenarios from LEO showed that if intensities from horizon-to-horizon sky scans at several latitudes were available (rather than radially outward views), then parameters could be retrieved with much higher fidelity ($R \cong \hat{I}$). This conclusion only applies to the STP nighttime observations. LEO observations during the day contain large contributions from the topside ionosphere.

8. Multi-point Measurements

In anticipation of future global imaging missions, we have extended this work to investigate the advantages of multi-point measurements of the plasmasphere. For this initial study, we consider three configurations: two spacecraft at high (5.6 Earth radii) and low (1000 km) orbital altitudes (HILO), two spacecraft at high altitudes (HIHI) and two at low altitudes (LOLO). The HILO configuration places the satellites at 90° from the Earth-Sun direction over the North Pole. Sky scans with a hypothetical EUV sensor are examined for planes parallel (0 h solar time; Figure 6a) and perpendicular (18 h solar time; Figure 6b) to the Earth-Sun direction. (We define a scan as an “observation” every two degrees of angle from local vertical through nadir in the plane.) Analysis of these two cases allows a comparison of the information content of the sunlit plasmasphere and the shadowed plasmasphere. Each of the HIHI and LOLO cases position a satellite over the North Pole, with the second at 20° latitude in the midnight meridian (not shown in Figure 6). All scans for the latter two cases are made in the Sun-Earth-Satellite plane.

First, we invert and analyze the information content of observations from each satellite location separately. We then invert the combined data sets from two-satellite combinations for each of the three cases to judge the value added for multi-point viewing. To reduce the effect of “instrumental” noise on the retrieved parameters, the sensitivity is initially set at 10^5 counts per Rayleigh. We begin by studying the high altitude satellite observations individually. For the high altitude satellite in the HIHI case, the model resolution matrices, R , equal \hat{I} for both the 18 h (Figure 6a) and the 0 h (Figure 6b) scans; consequently no additional information is available from scanning through the shadow. In fact, the lower intensities observed in the midnight plane cause the model parameters to be retrieved with less precision than in the 18 h case. As an additional test of the 0 h observation, we relocate the Sun to the Northern hemisphere (sub-solar latitude of 20° N). Then variances of the parameters increase significantly due to higher intensities produced when more of the plasmasphere is illuminated above the shadow. Next we consider the high altitude satellite at 20° latitude in the midnight meridian (one of the high altitude satellites in the HIHI case). The model resolution matrix in this case departed significantly from \hat{I} for the three parameters describing the height variation of He^+ , demonstrating that those parameters could not be retrieved from the observations. Even so, the plasmopause L-shell could still be retrieved with high fidelity. We conclude from this examination of data from single satellite locations at high altitudes, that the ability of a sensor to retrieve model parameters, and the precision of those parameters depends critically on satellite location and viewing directions relative to the Sun.

As expected, model parameter uncertainties in all cases were lower when “observations” from two satellites were inverted together. Once it was established that the parameters could be retrieved ($R = \hat{I}$), the overriding factor governing parameter precision becomes counting statistics. Reducing the “instrumental” sensitivity to a more reasonable

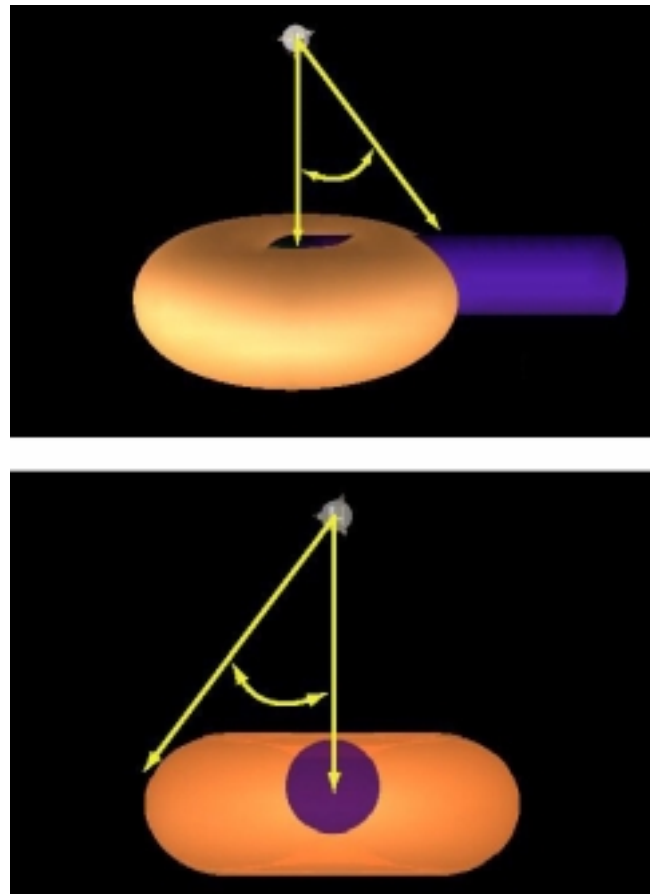


Figure 6. (a) Upper panel: Observational configuration for high altitude satellite in HILO case. The satellite is at 90° latitude and $5.6 R_E$ altitude. The local time of the scan is 0 h. (b) Lower panel: As in (a) but with local time.

100 counts per Rayleigh has no effect on the model resolution matrix. Of course, model parameter uncertainties are worse than for 10^5 counts per Rayleigh. Even so, propagation of the parameter uncertainties into He^+ density uncertainties lead to less than 20% error for altitudes above about 1.6 Earth radii (at least for the 18 h scan from high altitude). We conclude that for the parameterized model chosen, reasonable precision can be obtained in the retrieved helium ion densities.

9. EUV Discussion and Summary

In all cases examined in this study, the plasmopause L-shell parameter could be retrieved with good fidelity. Thus, future imaging mission should be able to discern discrete features such as plasma “blobs” or sunward-directed streamers, from the plasmopause. One remarkable extant example is the observation from the STP 72-1 satellite of sunlit He^+ outside the plasmopause, well beyond the Earth shadow [Meier et al., 1998].

Within the plasmasphere, parameters describing the density variation along L-shells exhibit the largest uncertainties and the poorest retrievability. To some extent, that is a property of the parameterized function used to describe the ion densities. An improved description of the plasmasphere whose analytic functionality is more closely tied to plasmaspheric physics might provide better parameter retrievability. One model based on kinetic theory [Reynolds et al., 1997] will be investigated in future work. A newer version of the Reynolds et al.

model uses a parameterized global electric field to characterize the plasmapause [Reynolds et al., 1998], raising the prospect of direct electric field retrieval from EUV image inversion. We will also investigate an alternative model, called the concentration scalar model (CSM; Picone et al. [1997]), in which the model parameters consist of the individual He^+ densities mapped onto a plasmaspheric grid. Like true tomography in which densities are constant within altitude-latitude cells, the CSM facilitates identification of which plasmaspheric regions contribute to the information received by an EUV sensor.

In summary, we have found in this study that: 1) the STP 72-1 EUV remote sensing observations of the plasmasphere from LEO can be fit with a simple parameterized model, but the observing scenario was insufficient to retrieve model parameters with fidelity, 2) multiple satellite observations improve the retrievability of model parameters, 3) observations from high altitudes away from the Earth shadow are sufficient to retrieve model parameters, but 4) the precision of the retrieved parameters depends in turn upon the measurement precision, and 5) the parameterized model of Meier et al. [1998] is limited in scope; improved models with good physical basis could lead to much better EUV image inversion.

10. Tomography

A clear advantage of a multi-spacecraft neutral atom imaging missions is the potential for tomographic reconstruction of the spatial distribution of the plasma. As a result of IMAGE intensive research over the past few decades, e.g., medical [Cormack, 1964] and thermonuclear fusion [Shore and Johnson, 1980; Holland and Navratil, 1986], an extensive body of literature concerning tomographic reconstruction techniques exists. Computer Aided Tomography (CAT) scans and Positron Emission Tomography (PET) scans rely on a combination of highly collimated fields of view, a large number of lines-of-sight (100's to 1000's), and computationally intensive reconstruction algorithms to achieve the high spatial resolutions required for medical imaging. To acquire data from enough lines-of-sight to tomographically reconstruct the large scale spatial distribution of plasma in the magnetosphere, one could either fly tens of spacecraft or use the orbital motion of a single spacecraft to acquire a sufficient number of different lines-of-sight. The penalty for using a single spacecraft is the loss of time resolution - a key parameter in magnetospheric imaging. The same compromise has been made in medical imaging. CAT scanners typically use a single source-detector pair and move them around the patient to acquire approximately 1000 lines-of-sight for high spatial resolution and poor temporal resolution. On the other hand, PET scanners image metabolic processes with modest spatial resolution and excellent time resolution by using a few hundred detectors simultaneously.

The spatial resolution of tomographic reconstruction is constrained by the number of independent measurements of the emission region. In other words, to divide up a slice of the magnetosphere into 100 "pixels" requires a hundred or more views through the emission region [Hutchinson, 1987; Chartas and Hokin, 1992]. Ten spacecraft in the same orbital plane but out of phase from each other would speed up the process by an order of magnitude, yielding a time resolution of a tenth of the orbital period. However, spatially and temporally resolved measurements of the entire magnetosphere would require a prohibitively large number of spacecraft. Because neutral atom images are distinct from photon based images in that the information is carried at sub-light velocities, a modest constellation of spacecraft in a single orbital plane could still generate spatially resolved information about distant plasma regions, e.g. the extended plasma sheet in the magnetotail.

11. Finite Transit Location Technique

The finite transit time of medium energy (less than 10 keV) neutral atoms across the magnetosphere is sufficient to permit the use of triangulation to spatially localize transient events. For example, assuming a cloud of plasma with a 2 keV temperature is injected into the plasmasheet at $30 R_E$. For two spacecraft in a hypothetical dawn-dusk, $6 R_E$ circular polar orbit separated by one fourth of an orbital period, the difference in arrival times for 1 keV neutral hydrogen atoms is approximately 3 minutes (see Figure 7). The current generation of neutral atom imagers [Burch et al., 1997] is optimized for high angular resolution and modest temporal resolution (roughly five minute sample intervals). Minor modifications of onboard acquisition software would permit data collection for shorter intervals at the expense of less angular resolution in order to obtain sufficient signal for triangulation purposes. Thus the location of injection events in the magnetotail could be localized to within an R_E , providing both qualitative and quantitative information from the neutral atom images.

12. Conclusions

The progress we have made in deconvolving multiple vantage point magnetospheric images has guided our efforts in defining multipoint magnetospheric imaging missions. In particular, we have found that multiple vantage points can greatly improve the fidelity of the reconstructed ion distributions.

However, we have also found that not all combinations are created

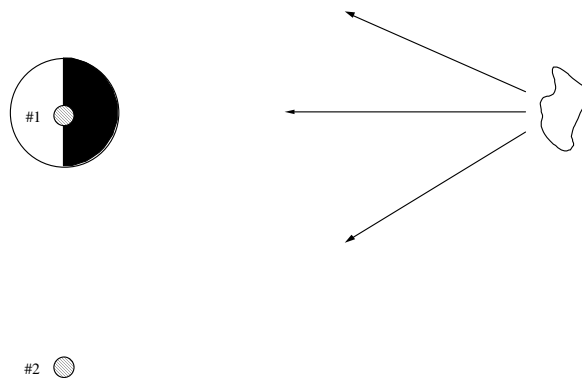


Figure 7. Medium energy neutral atom fluxes obtained by two spatially separated spacecraft can be used to triangulate the position of deep tail injection events as a result of the finite transit time of the neutral atoms.

equal. LEO vantage points, especially at high latitude, are shown to be very powerful in combination with high altitude imaging. The addition of third and fourth vantage points are beneficial, but primarily in assuring that at least two of them are in non-degenerate, high information content positions. Tomographic techniques may be useful if a sufficiently large number of imagers is flown. High angular resolution, and high sensitivity, are shown to be as important as additional vantage points (beyond 2).

Although the study is not yet concluded, it is highly probable that a constellation of LEO and high altitude spacecraft will be the most valuable combination. A minimum of one spacecraft in each orbit is required, but additional spacecraft (up to 4 in LEO and 2 to 3 at high altitude) would significantly improve coverage from optimal positions. Although more ambitious, a large constellation would permit a tomographic approach (without time-aliasing).

References

- C:son Brandt et al., submitted to JGR, 1998.
- Carpenter, D. L., *EOS*, 9, 89, 1995.
- Chartas, G. and S. A. Hokin, *Phys. Fluids B* 4, 4019 (1992)
- Chase et al., JHU/APL Tech. Dig., 16, 111, 1995.
- Cormack, A.M., *J. Appl. Phys.* 35, 2908 (1964).
- Craven, P.D. D. L. Gallagher, and R. H. Comfort, Relative concentration of He⁺ in the inner magnetosphere as observed by the DE 1 retarding ion mass spectrometer, *J. Geophys. Res.*, 102, 2279, 1997.
- Henderson et al., *Geophysical Research Letter*, 24, 1167, 1997.
- Holland A. and G.A. Navratil, *Rev. Sci. Instrum.* 57, 1557 (1986).
- Horwitz, J. L., R. H. Comfort and C. R. Chapell, A statistical study of plasmasphere density structure and boundary locations, *J. Geophys. Res.*, 95, 7937, 1990.
- Hutchinson, I. H., *Principles of Plasma Physics*, Cambridge University Press, New York, 1987.
- Johnson C. Y., J. M. Young, and J. C. Holmes, Magnetoglow: a new geophysical resource, *Science*, 171, 379, 1971.
- Lui et al., *Geophys. Res. Lett.*, 23, 2641, 1996.
- Meier, R. R., A. C. Nicholas, J. M. Picone, D. J. Melendez-Alvira, G. I. Ganguli, M. A. Reynolds and E. C. Roelof, Inversion of plasmaspheric EUV remote sensing data from the STP 72-1 satellite, *J. Geophys. Res.*, 103, 17505, 1998.
- Menke, William, *Geophysical Data Analysis: Discrete Inverse Theory*, International Geophysics Series, No. 45, Academic Press, London, 1989.
- Newberry, I. T., R. H. Comfort, P. G. Richards, and C. R. Chappell, Thermal He⁺ in the plasmasphere: comparison of observations with numerical calculations, *J. Geophys. Res.*, 94, 15265, 1989.
- Picone, J. M., R. R. Meier, O. A. Kelley, R. J. Thomas, K. F. Dymond, and R. P. McCoy, Investigation of ionospheric O⁺ remote sensing using the 834 Å airglow, *J. Geophys. Res.*, 102, 2441, 1997b.
- Reynolds, M. A., G. Ganguli, J. A. Fedder, and D. J. Melendez-Alvira, Effect of diurnal convection on trapped thermal plasma in the outer plasmasphere, *Geophys. Res. Lett.*, 24, 2255, 1997.
- Reynolds, M. A., G. Ganguli, J. A. Fedder, J. Lemaire, R. R. Meier and D. J. Melendez-Alvira, Thermal plasma morphology: Effect of geomagnetic and solar activity, *Geophys. Res. Lett.*, submitted for publication, 1998.
- Roelof et al., *J. Geophys. Res.*, 90, 10911, 1985.
- Roelof et al., *Proc SPIE*, 2008, 202, 1993.
- Roelof, *Adv. Space Res.*, 9(12), 195, 1989.
- Roelof, E. C. and A. Skinner, *Space Sci. Rev.*, submitted, 1998.
- Roelof, E. C., *Adv. Space Res.*, 20(3), 341-350, 1997a
- Roelof, E. C., *Adv. Space Res.*, 20(3), 361-366, 1997b
- Roelof, *Geophys. Res. Lett.*, 14, 652, 1987.
- Roelof, *Adv. Space. Res.* 20, 341, 1996
- Shore, J.E., and R.W. Johnson, *IEEE Trans. Inf. Theory* 11-26, 26 (1980).
- Tarantola, Albert, *Inverse Problem Theory*, Elsevier, Amsterdam, 1987.
- Williams, D. J., E. C. Roelof, and D. G. Mitchell, Global magnetospheric imaging, *Rev. Geophys.* 30, 183, 1992.

B. H. Mauk, D. G. Mitchell, E. C. Roelof, The Johns Hopkins University, Applied Physics Laboratory, Johns Hokins Road, Laurel, Maryland 20723-6099. (e-mail: don.mitchell@jhuapl.edu)

H. O. Funsten, D. J. McComas, Space and Atmospheric Sciences Group, MS D466, NIS-1, Los alamos National Laboratory, Los Alamos, NM 87545.

M. Gruntman, Space Sciences Center, Stauffer Hall of Science 274, MC-1341, University of Sourthern California, Los Angeles, CA 90089-1341.

M. Hesse, NASA, Goddard Space Flight Center, Code 696, Greenbelt, MD 20771.

R. R. Meier, Center of Space Research, Naval Research Laboratory, Code 7640, Washington, D.C. 20375.

E. E. Scime, West Virginia University, Physics Department, Morgantown, WV 26506.

